Biosensors and Bioelectronics 74 (2015) 16–23

Contents lists available at ScienceDirect

Biosensors and Bioelectronics

journal homepage: www.elsevier.com/locate/bios

Quantum dots decorated gold nanorod as fluorescent-plasmonic dual-modal contrasts agent for cancer imaging

Qiong Wu [1], Lu Chen [1], Liang Huang, Jing Wang, Jiawei Liu, Chao Hu, Heyou Han *

State Key Laboratory of Agricultural Microbiology, College of Science, Huazhong Agricultural University, Wuhan 430070, PR China

ARTICLE INFO

Article history:
Received 10 March 2015
Received in revised form
6 June 2015
Accepted 6 June 2015
Available online 11 June 2015

Keywords:
Gold nanorod
Quantum dots
Amphiphilic organosilica
Fluorescence
Dark-field
Dual-modality imaging

ABSTRACT

Constructing integrative optical bioprobe with both fluorophores and plasmonic functional groups is of particular interest in precise co-localized bio-imaging probe development. Herein, we fabricated a novel hierarchical complex nanoparticle with fluorescent and plasmonic components spatially separated, which is composed of highly brilliant CdSe/CdS/ZnS QDs decorated gold nanorod (AuNR) with silicon coating. This complex structure served as an efficient dual-modality imaging contrast agent, where the potential fluorescence resonance energy transfer (FRET) between QDs and AuNR was avoided by the intermediate silica layer as well as minimized spectral overlap between QDs and AuNRs. The high-density loading of QDs was achieved by thiol-metal affinity driven assembly of hydrophobic QDs with thiolated AuNR@SiO_2 substrate, which is able to show a strong fluorescence emission. After amphiphilic organosilica-mediated phase transferring and functionalization with transferrin (Tf), these nanoparticles entered A549 cells and exhibited high contrasting fluorescent and dark-field signals for co-localized cancer cells imaging. The results demonstrate that these nanoparticles are potential candidates as dual modal probes for fluorescence and dark-field image.

1. Introduction

The recent progress of nanotechnology has provided numerous functional nanoparticles with unique and tuneable optical, magnetic and electronic properties, which reveal great potential in biomedical diagnostics (Huang et al., 2009; Michalet et al., 2005; Gao et al., 2009) compared with traditionally used contrasting agents. Meanwhile, the usage of nanoparticles as biomedical label became an advantage for significantly enhanced signal to noise ratio and engineerable surface chemistry as well as in vivo circulating dynamics (Song et al., 2010; Tian et al., 2013). Encouragingly, the integration of discrete inorganic functionalities at the nanoscale offers a new opportunity for multi-modality diagnostics, breaking through the distinct limitations of their single-modality counterparts, in terms of a precise comparative analysis and the elimination of organism background interference (Jin et al., 2010; Mulder et al., 2005).

Semiconductor quantum dots (QDs) and AuNR are two emerging classes of fluorescence and light scattering probes, exhibiting high quantum yield/scattering efficiency and facile tunability in size, shape and emission/localized surface plasmon resonance (LSPR) absorption (Pérez-Juste et al., 2005; Chen et al., 2013; Resch-Genger et al., 2008). The combination of the two components is potentially powerful in precise identification of subcellular targets by co-localization of fluorescent (Gao et al., 2004) and light scattering (dark field) imaging (Ding et al., 2007). The composite of QDs and AuNR has proved to be an excellent multi-modality imaging probe in vivo that exhibited great potential in biological and medical applications. Nevertheless, the integration of a fluorophore with plasmonic material has been a great challenge (Jin and Gao, 2009), considering the largely or entirely quenching of fluorescence by the absorber (Shi et al., 2006; Li et al., 2011). On the other hand, the high sensitivity of QDs fluorescence to their native surface passivation (by organic ligands) raises another obstacle (Koole et al., 2008), in fabricating water soluble QDs and their derivative composite structures with well-preserved fluorescence emission. Although fluorescence enhancement by QDs and AuNR is highly technical, many efforts are still made to fabricate new composite that have both enhanced fluorescence and scattering properties. For example, Nepal et al. have fabricated an assembly of quantum dots on gold nanorod with precisely controlled spacing, quantum dot/nanorod ratio, and long-term colloidal stability by a bottom-up approach (Nepal et al., 2013). Zhao et al. have developed a folic acid-conjugated silica-coated gold nanorodsand quantum dots probe for dual-modality CT and fluorescence imaging and photothermal therapy (Xia et al., 2014). The results have shown that the probe composed of QDs and AuNR exhibited great potential for target tumor imaging and therapy. Xiong et al. have demonstrated a

* Corresponding author.
E-mail address: hyhan@mail.hzau.edu.cn (H. Han).
[1] Qiong Wu and Lu Chen contributed equally to this work.

http://dx.doi.org/10.1016/j.bios.2015.06.010
0956-5663/

plasmon enhanced fluorescence mechanism by monolayers that make quantum dots on vertically aligned gold nanorod (Peng et al., 2014). In this present work, it has been designed a novel engineered nanoparticle which realized both superior performance and good compatibility of QDs and AuNR excellent functionalities for cancer cells dual modality image.

The high efficient assembly of hydrophobic QDs with metal-affinity substrates via coordination chemistry (Lu et al., 2011), provides a promising alternative to improve QDs loading density and optical properties (Jun et al., 2012), compared with aqueous phase layer-by-layer assembly technics (Bakalova et al., 2008). Silicon, a versatile and biocompatible material for both substrates and coating layers on nano-objects (Jana et al., 2007; Foda et al., 2014), exhibits unique process ability that enabling facile incorporation of noble metal nanoparticles and a variable space between the plasmonic interior and surface attached fluorophores (Liu and Prall, 2006). In this regard, the metal-affinity assembly based hierarchical complex of QDs and AuNR using silica as intermediate layer, appears advantageous than previously established AuNR based composite structures, especially in improved fluorescent brightness of single composite particle (Zhu et al., 2012; Huang et al., 2012) and tunable distance to avoid potential energy transfer between the donor–acceptor pair (Pons et al., 2007; Xia et al., 2011).

Herein, we explored a novel silica based multifunctional nanoplatform integrated with AuNR and compact/highly fluorescent QDs layer for fluorescence and dark-field co-localized cancer cells imaging. As illustrated in Scheme 1, the AuNR embedded silica particles with thiolated surface were employed as composite metal-affinity substrates, to assembly directly with hydrophobic CdSe/CdS/ZnS QDs in organic phase, achieving both high fluorescence and particle packing density. The water solubilization of such hydrophobic assembly was realized by organosilica encapsulation and silicate deposition, in favor of a homogeneous silica shell formation and preserved optical properties. The surface of this composite particle was functionalized with transferrin via a polyethylene glycol (PEG) linker and properly passivated by inert PEG chains for a dual-modal imaging probe fabrication.

2. Experimental sections

2.1. Materials and chemicals

Cetyltrimethylammonium bromide (CTAB), cadmium oxide (CdO), oleic acid (OA), 1-octadecene (ODE), tributyl phosphine (TBP), oleyl amine, tetraethyl orthosilicate (TEOS), (3-mercaptopropyl) trimethoxysilane (MPS), sodium silicate solution (27 wt% SiO_2), 3-aminopropyl triethoxysilane (APTES) and transferrin (Tf) were purchased from Aldrich. N-octyltrimethoxysilane (OTMS) and zinc acetate were obtained from Alfa Aesar. NHS-PEG_{5000}-OCH_3 and NHS-PEG_{5000}-Mal were acquired from NANOCS. Tetrachloroauric acid ($HAuCl_4 \cdot 3H_2O$), sodium borohydride ($NaBH_4$), silver nitrate ($AgNO_3$), ascorbic acid (AA) and ammonia aqueous solution (25 wt%) were supplied by Sinopharm Chemical Reagent Co., Ltd. Ultrapure water with a conductivity of 18.25 MΩ cm was used throughout the experiments. The details of preparation processes for CdSe/CdS/ZnS QDs and thiolated AuNR@SiO_2 substrates are given in the Supporting information.

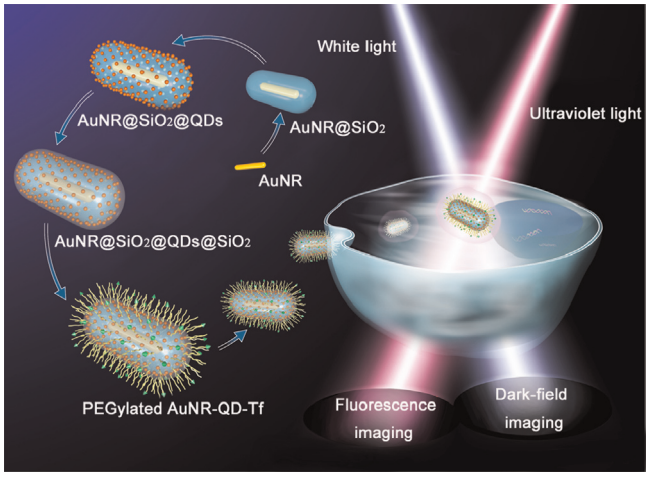

Scheme 1. Schematic illustration for the preparation of PEGylated AuNR-QDs-Tf bioconjugates for fluorescence and dark-field dual-modal targeted cellular imaging.

2.2. Preparation of AuNR@SiO_2@QDs@SiO_2 hierarchicalcomplex

For assembling with CdSe/CdS/ZnS QDs, 2.4 mL of QDs (3 mg mL^{-1}) toluene solution was added into the wet precipitate of thiolated AuNR@SiO_2 (corresponding to 0.08 nmol AuNRs) and sonicated for 30 min. The AuNR@SiO_2@QDs assemblies were collected by centrifugation and then washed with toluene to remove excess QDs. The precipitate was properly dried under air flow and dissolved in 0.24 mL of OTMS with the aid of ultrasonication. Then the fluid was supplemented with 16 mL methanol and 0.4 mL ammonia aqueous solution. The phase transfer of AuNR@SiO_2@QDs assemblies was performed by sonicating the above mixture for 30 min, followed by centrifugating and washing the precipitate with methanol to remove excess OTMS. Finally, the silanized AuNR@SiO_2@QD assemblies (equivalent to 0.08 nmol AuNRs) were dispersed in 40 mL water, 40 μL sodium silicate solutions and 40 μL ammonia aqueous solution, stirred at room temperature for at least 12 h to deposit a thin silica layer, and AuNR@SiO_2@QDs@SiO_2 nanocomposites were obtained.

2.3. Bioconjugation of AuNR@SiO_2@QDs@SiO_2 nanoparticles

Two milliliter precipitate of AuNR@SiO_2@QDs@SiO_2 (corresponding to 0.01 nmol AuNRs) was dispersed in a solution of 2 mL ethanol and 2 μL APTES, followed by stirring for 12 h at room temperature. Then the mixture was collected by centrifugation, the fabricated nanoparticles denoted as AuNR-QDs-NH_2. Subsequently, all the pellets of AuNR-QDs-NH_2 were rinsed twice, and then dispersed inanhydrous DMF. The as-prepared dispersion was supplemented with 6 mg of NHS-PEG (NHS-PEG_{5000}-OCH_3: NHS-PEG_{5000}-Maleimide = 4:1) and 40 μL of anhydrous triethylamine. The resulting solution was stirred for 8 h to obtain AuNR-QDs-PEG which was washed with DMF and water, and then resuspended in 2 mL sodium borate buffer (50 mM, pH 9.18). Finally, the as-prepared dispersion was amended with 100 μL transferrin (2 mg mL^{-1} in 50 mM NaCl solution), followed by gentle stirring for 12 h at room temperature, and then PEGylated AuNR-QDs-Tf NPs were obtained.

2.4. Cell culture and cytotoxicity test

A549 cells were seeded in a 96-well plate at a density of 1×10^5 cells per well in DMEM plus 10% FBS at 37 °C under 5% CO_2. After cultured for 24 h, the cells attached to the plates were supplemented with different concentrations of PEGylatedAuNR-QDs-Tf NPs and then incubated at 37 °C under 5% CO_2 for 48 h. The concentrations of the NPs were 0.05, 0.1, 0.2, 0.28, and 0.36 nM (calculated from the concentration of AuNRs), respectively. At the end of the incubation, the media containing the PEGylated AuNR-QDs-Tf was removed, and 10 μL 3-(4, 5-dimethylthiazol-2-yl)-2, 5-diphenyltetrazolium bromide (MTT) solution (5 mg mL^{-1}) was added and incubated for additional 4 h. After that, the medium

containing MTT was discarded and replaced with 100 μL dimethyl sulfoxide (DMSO) per well. The absorbance was recorded (λ=490 nm) by a microplate reader. Cells cultured without PEGylated AuNR-QDs-Tf were used as a control.

2.5. TEM imaging of PEGylatedAuNR-QDs-Tf exposed cells

Cells were seeded in 6-well plates at a density of 5×10^5 cells per well at 37 °C under 5% CO_2. After cultured with a medium containing 0.2 nM PEGylated AuNR-QDs-Tf for 24 h, the NPs that were not taken up by the cells were discarded, and the cells were washed with PBS buffer (0.1 M, pH 7.4). Then the cells were scraped from the plates and centrifuged at 1500 rpm for 5 min. The collected cell pellets were fixed with 2.5% glutaraldehyde for 4 h at room temperature. After the cell pellets were re-dispersed in fixatives, a drop of as-prepared solution was placed on the copper grid. After absorption for 10 min, the copper grid was rinsed with PBS (0.1 M) and post-fixed in 1% osmium tetroxide solution for 30 min. After post fixation, the copper grid was rinsed with PBS (0.1 M), dehydrated in a graded series of ethanol (50%, 70%, 80%, 90%, 95% and 100%), and embedded in Epon/Araldite resin. Ultrathin sections (50–70 nm) were obtained with an ultramicrotome and examined by TEM.

2.6. Dual-modal targeted cellular imaging

The fluorescence images and dark-field images were recorded on the same optical microscope (Zeiss Axio Imager A1). The cells were cultured at 37 °C under 5% CO_2 on 14 mm diameter glass cover slips in 12-well plates at a density of 1×10^4 cells per well. Next, the cells were supplemented with PEGylatedAuNR-QDs-Tf to a final concentration of 0.2 nM and then incubated in the fresh medium for 24 h. After incubation, the cells on each cover slip were washed with PBS and sealed with a small amount of glycerol. Fluorescence imaging was performed by using ultraviolet to irradiate the cell samples and the objective to collect the fluorescence signals. Co-localized dark-field imaging was accomplished by changing the irradiation source and manipulating the dark-field imaging accessory, and the tungsten lamp with a narrow beam of white light was employed to irradiate the cell samples. Meanwhile, the scattering light signals were collected from the same samples by the same objective.

2.7. Characterization

TEM images were taken using a JEM-2010FEF transmission electron microscope operating at 200 kV. Absorption of the samples was recorded on the Nicolet Evolution 300 UV–vis spectrometer. The photoluminescence (PL) spectra and lifetime analysis were carried out using an Edinburgh FLS920 spectrometer with an integrating-sphere attachment under excitation of 390 nm. Measurements of zeta potential were acquired on a Malvern Zetasizer Nanoseries. X-ray photoelectron spectroscopy (XPS) was recorded by a Thermo VG Multilab 2000 spectrometer equipped with a monochromatic Al Ka radiation source.

3. Results and discussion

3.1. Synthesis and characterization

In order to obtain robust and high-performance fluorescent-plasmonic nanocomposites, the AuNRs were coated with a dense layer of silica, mediated by an initial mesoporous silica layer. The composite substrate was functionalized with thiol groups, followed by high-efficient assembly with hydrophobic QDs in organic phase. The phase transfer was realized by amphiphilicsilane encapsulation and silica deposition. The biocompatibility and active targeting of the composites were achieved by surface grafting with PEG linkers and conjugation with transferrin, as illustrated in Fig. 1. Highly monodispersed AuNRs with an average aspect ratio (length/diameter) of approximately 3.5 were synthesized by seed-mediated approach (Nikoobakht and El-Sayed, 2003) (Fig. 2a). Since AuNRs are prone to aggregate as well as they have a serious quenching effect on proximal QDs fluorescence through energy transfer (Li et al., 2009), a homogeneous layer of mesoporous silica about 15 nm was initially coated on AuNR to form AuNR@mSiO_2 (Fig. 2b) with base-catalyzed hydrolysis and condensation of silanes, where the CTAB micelles served as an organic template. In order to achieve high-density surface thiol groups for efficient assembling, a compact silica layer was further deposited according to a previously reported procedure (Gorelikov and Matsuura, 2007), forming a conjugate namely AuNR@SiO_2 (Fig. 2c). By controlling the concentration of AuNR@mSiO_2 and the hydrolysis of TEOS, the tunable compact silica shell could be prepared. In this case, the thickness of the silica layer was about 55 nm in total. To

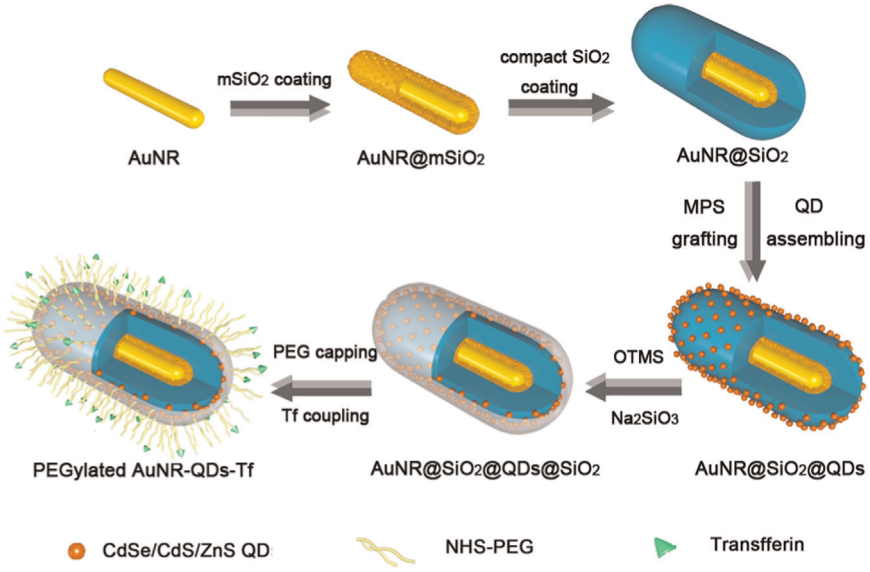

Fig. 1. Design strategy and synthetic route of bio-conjugated nanoprobe PEGylated AuNR-QDs-Tf.

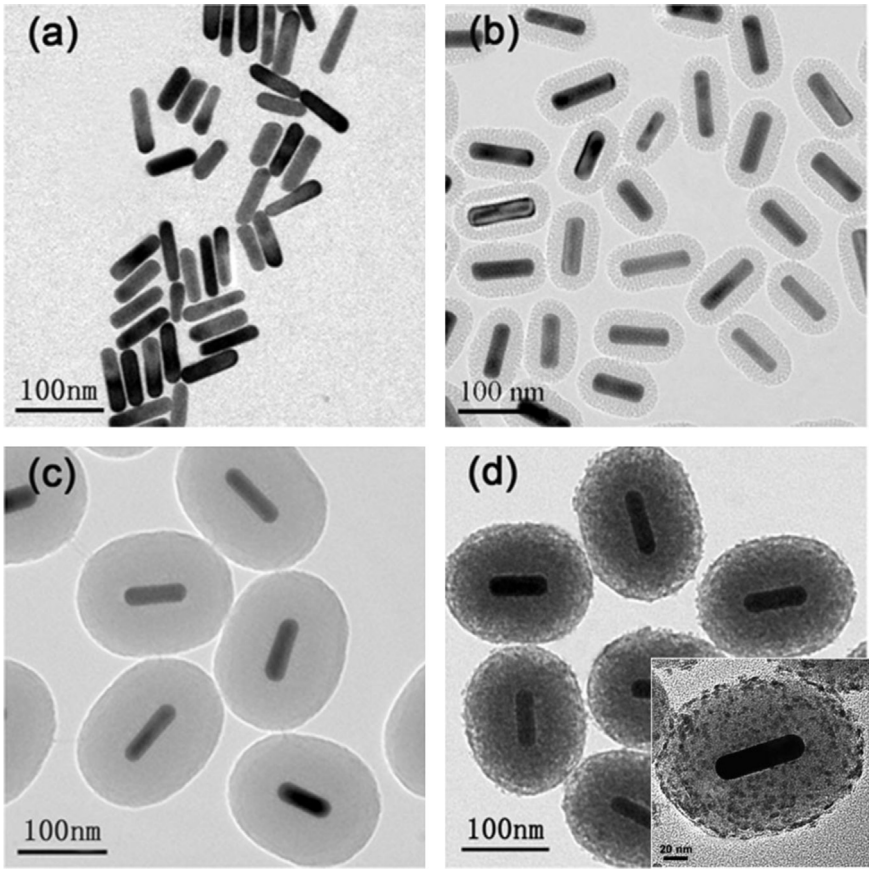

Fig. 2. TEM images of (a) AuNR, (b) AuNR@mSiO$_2$, (c) AuNR@SiO$_2$ substrates, and (d) AuNR@SiO$_2$@QDs@SiO$_2$ nanocomposites (inset: enlarged image of a single particle).

enhance hydrophobicity in nonpolar solvents and to improve assembly efficiency in organic phase via thiol-metal coordination, we grafted AuNR@SiO$_2$ substrates with mercaptopropyl groups. Afterwards, an excess amount of QDs dispersed in toluene was injected into the wet thiolated-AuNR@SiO$_2$ precipitate to ensure dense coverage. The high-efficient thiol-metal coordination driven assembly produced the surface saturated AuNR@SiO$_2$ composites by QDs. Finally, the hydrophobic assemblies underwent an ultrasonic assisted silanization with OTMS forming amphiphilic silanetriols for transferring into aqueous phase. After silicate deposition, the water-soluble AuNR@SiO$_2$@QDs@SiO$_2$ nanoparticles with high QDs loading and good monodispersity were formed as illustrated in Fig. 2d.

The key to construct multimodal optical nanoprobe is retaining the unique optical property of each component after nanoscale integration. As AuNR can quench the fluorescence of proximal fluorophores, combining high-quality QDs with plasmonic materials like AuNRs is challenging. To avoid potential fluorescence resonance energy transfer (FRET) between QDs and AuNRs, in addition to control the thickness of silica layer between QDs and AuNRs (>10 nm), it should make the emission spectrum of QDs and the plasmon absorption spectrum of AuNRs separated. As shown in Fig. 3a, the as-prepared AuNRs had a longitudinal surface plasmon resonance (SPR) peak at 780 nm and an absorption valley at 625 nm, which was chosen to minimize the spectra overlap with QDs (emission wavelength of 630 nm). An obvious red-shift ($\sim$15 nm) of the absorption spectra was observed for AuNR@SiO$_2$, which could be attributed to an increase in the local refractive index of the medium surrounding AuNRs (Wu and Xu, 2009). It is worth noting that the prepared AuNR@SiO$_2$@QDs@SiO$_2$ nanocomposites maintained original plasmon resonance absorption feature of AuNRs. The organosilica/silica bilayer coating on these hydrophobic assemblies favored a high retention of QDs PL properties, which is advantageous than most used ligand exchange based silica coating strategies. As shown in Fig. 3b, after a temporary PL degradation, the fluorescence intensity was doubled after 12 h active silica deposition, and stabilized after 48 h deposition. The recovering behavior was probably caused by the accomplishment of silanol condensation and silica shell growth around QDs, which effectively isolated them from external aqueous environment. The fluorescence spectra of the QDs incorporated in the hierarchical structure was nearly the same with those QDs in oil phase (Fig. 3c).

Time-resolved photoluminescence was carried out to confirm the retention of QDs PL properties. As illustrated in Fig. 3d, the fluorescence decay curve of AuNR@SiO$_2$@QDs@SiO$_2$ NPs was almost identical to that of CdSe/CdS/ZnS QDs. The same result could be found in the fitting parameters as listed in Table S1. The data indicated that the potential FRET between QDs and AuNR did not happen, as the fast decay component showed tiny changes (Fan et al., 2010) and the lifetime of the QDs incorporated into AuNR@SiO$_2$ substrate was longer than 1 ns (Ito et al., 2007), which was attributed to the existence of the thick silica spacer and the spectral separation. In addition, it definitely indicated a good retention in QDs PL emission because of the preserved original ligands from amphiphilic organosilica interlayer. The prepared hybrid AuNR@SiO$_2$@QDs@SiO$_2$ nanocomposites maintained the intrinsic optical property of both AuNR and QDs, revealing their great potentials as multimodal imaging and diagnostics agent.

Water solubility is a very important consideration when NPs are used for bio-application. A previous study reported that for bigger NPs (>50 nm), the wrapping time is slower because of slower receptor diffusion kinetics, resulting in a smaller number of NPs being taken up (Nativo et al., 2008). Meanwhile, precipitation occurred after the solution was left at room temperature for a few days, as the

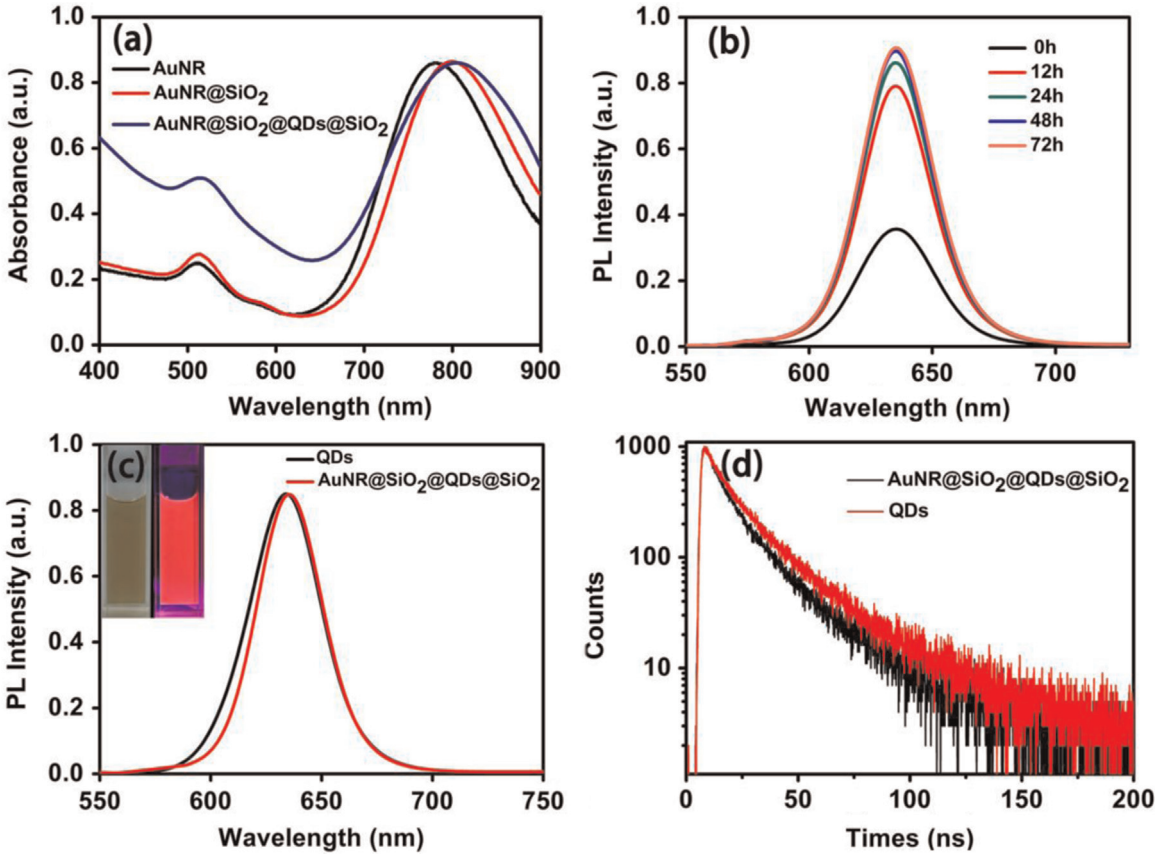

Fig. 3. (a) UV–vis absorption spectra of AuNRs, AuNR@SiO_2 substrates and AuNR@SiO_2@QDs@SiO_2nanocomposites, (b) PL spectra of AuNR@SiO_2@QDs@SiO_2nanocomposites with different sodium silicate deposition time in aqueous phase, (c) PL spectra of CdSe/CdS/ZnS QDs and AuNR@SiO_2@QDs@SiO_2nanocomposites (inset: photographs of fluorescent nanocomposites aqueous solution under visible light and UV lamp), (d) PL decay curves of AuNR@SiO_2@QDs@SiO_2nanocomposites and CdSe/CdS/ZnS QDs.

PL intensity of the stock solution reduced (Fig. 4b). To increase water solubility, minimize nonspecific binding, and achieve high avidity to the target cells of the NPs, hetero-functional NHS-PEG_{5000}-maleimide/NHS-PEG_{5000}-OCH_3 and transferrin were used for the final functionalization on the outmost surface of AuNR@SiO_2@QDs@SiO_2, due to the ubiquitous nature of transferrin in humans with fewer immune responses. The nanoparticles fabricated as AuNR-QDs-NH_2 through APTES grafting were positively charged with a zeta potential of $\sim+25.3$ mV (Fig. S1, Supporting information) due to the amine surface functionality. The hierarchical complex with a biocompatible PEG-based composition were further fabricated using NHS-PEG_{5000}, which contained $\sim$20 wt% of maleimide for post-functionalizing with transferrin through Michael-addition reactions between the free lysines on the protein and the maleimide groups on the NPs (Wang et al., 2010) to facilitate the tracking of the nanoparticles in cells. The zeta potential of AuNR-QDs-PEG dropped to ~-14.2 mV, and with further transferrin functionalization, the PEGylated AuNR-QDs-Tf bioconjugates had a negative zeta potential of ~-20.1 mV to avoid nonspecific cell uptake (Gratton et al., 2008). Thechange in zeta potential primarily indicated that PEG chains and transferrin were successfully functionalized step by step.

The conjugation was further investigated by XPS. As shown in Fig. 4a, the binding energy (BE) of N_{1s} from AuNR-QDs-NH_2 was 399.5 eV. As expected, the concentration of oxygen increased by 4.89% assigned to PEG chains, implying that the AuNR-QDs-NH_2 was successfully PEGylated. In addition, AuNR-QDs-PEG displayed a photoemission at a BE of 399.7 eV belonging to N_{1s}. The higher binding energy may be due to the electron-withdrawing effect of the formed amido linkage via an amine-addition reaction between NH_2 and NHS groups. As for PEGylated AuNR-QDs-Tf, both the increase of nitrogen which changed from 0.53% to 1.02% and the appearance of a new element namely phosphorus (1.03%) in the NPs suggested that transferrin molecules were attached to the surface of AuNR-QDs-PEG. Another direct proof was shown by much stronger photoemission at a BE of 399.8 eV assigned to N_{1s}, this higher binding energy may be due to the increased electron-withdrawing effect of the formed broken delocalization bonds in the Maleimide groups during transferrin conjugation. In the process of conjugation, the relative elemental compositions of oxygen, nitrogen, and phosphorus increased, but the unrelative elemental compositions of cadmium and selenium decreased when compared with AuNR-QDs-NH_2 (Table S2, Supporting information). These confirmed PEG and transferrin were successfully attached onto the surface of AuNR@SiO_2@QDs@SiO_2 step by step.

To investigate the stability and biocompatibility of PEGylated AuNR-QDs-Tf NPs, we performed a photo-stability experiment by monitoring the time-dependent luminescent intensity of PEGylated AuNR-QDs-Tf NPs in PBS (Fig. 4b). The samples dispersed in PBS were excited at 390 nm and the emission signal was recorded every 12 h within the wavelength range from 550 nm to 750 nm. The result shows that fluorescence intensity was mainly consistent with the original value after 72 h, which suggested that the as-prepared NPs possessed good colloid stabilities after silica and PEG/transferrin capping.

3.2. Cytotoxicity and targeting ability of PEGylated AuNR-QDs-Tf bioconjugates to A549 cells

Although the bio-conjugates showed high optical performance and good water-solubility, the cytotoxicity of the NPs was supposed to be examined, as several factors such as concentration, size and the surface functional groups could lead to cell death

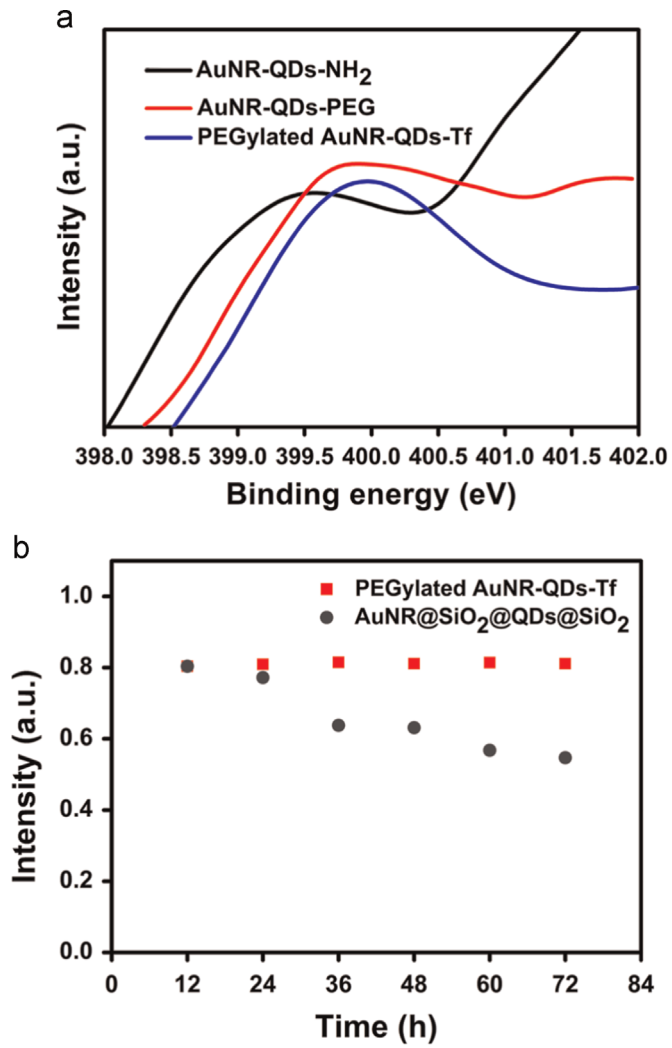

Fig. 4. (a) XPS characterization of N_{1s} of AuNR-QDs-NH_2, AuNR-QDs-PEG and PEGylated AuNR-QDs-TfNPs, (b) time-dependent luminescence intensity of AuNR@SiO_2@QDs@SiO_2 NPs and PEGylatedAuNR-QDs-Tf bio-conjugates in phosphate buffer solution (pH 7.4).

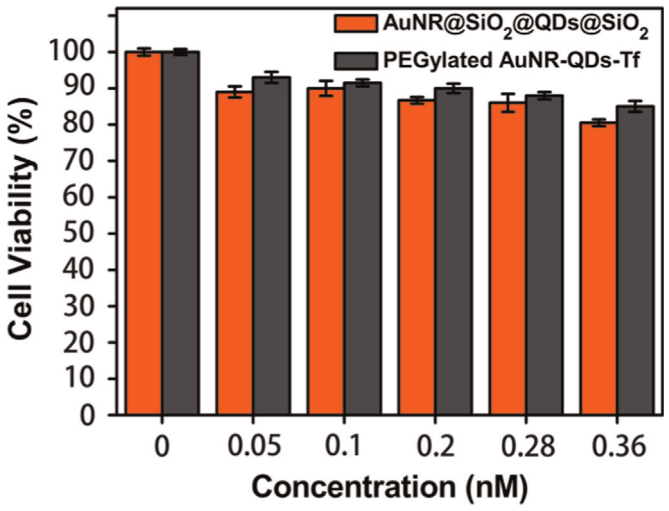

Fig. 5. Cell viability values (%) estimated by MTT proliferation tests versus incubation concentrations of AuNR@SiO_2@QDs@SiO_2 and PEGylated AuNR-QDs-Tf. Cells were incubated with 0.05–0.36 nM bio-conjugates at 37 °C for 48 h.

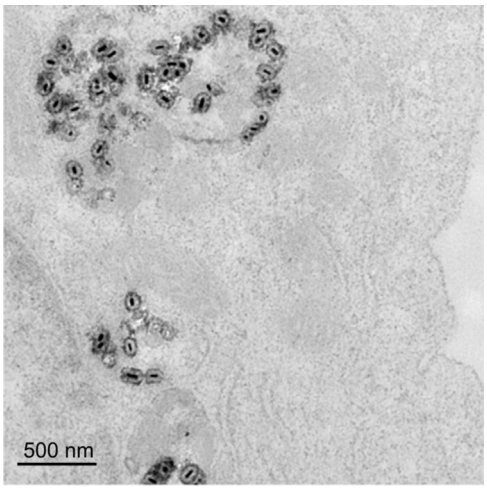

Fig. 6. TEM images of A549 cells with PEGylated AuNR-QDs-Tf NPs.

(Barreto et al., 2011). The unmodified AuNR@SiO_2@QDs@SiO_2 and bio-conjugated PEGylated AuNR-QDs-Tf cytotoxic effects on A549 cells were evaluated by performing MTT assays (Fig. 5). With the concentration of the unmodified and bio-conjugated NPs increased, no significant suppression of the cell viability was observed. Especially for PEGylated AuNR-QDs-Tf, the cell viabilities were estimated to be greater than 85% in the range of 0.05 nM to 0.36 nM, which confirmed that the nanocomposite had good biocompatibility and low cytotoxicity even though CdSe/CdS/ZnS QDs were embedded in the composite. This could be ascribed to the sufficient inorganic passivation by ZnS shell, together with effective protection by silica layers on QDs, leaving very fewer uncombined Cd^{2+} in the solution. Furthermore, we performed optical stability test of PEGylated AuNR-QDs-Tf in a cell culture medium. Fig. S2 demonstrates that no obvious PL intensity decrease was observed with excessive excitation for 1 h. Furthermore, the plasmon resonance absorption feature was nearly retained during 72 h intermittent measurement. The propaedeutic results demonstrate that PEGylated AuNR-QDs-Tf NPs may be a good dual-modal probe for further bio-imaging.

To monitor the cancer-targeted ability of PEGylated AuNR-QDs-Tf NPs, the cellular labeling was quantified by flow cytometry following the incubation with A549 cells and HEK 293 cells at different time (Fig. S3, Supporting information). Unlike the natural HEK 293 cells, the A549 cancerous cells treated by the bio-conjugated NPs show a higher occupation ratio and stronger signal at the same incubation concentration of 0.2 nM in each test point. With prolonging incubation time, the occupation ratio increased to 96.10% for A549 cells but only up to 10.85% for HEK 293 cells. The high occupation ratio in the cancerous cells group has shown that AuNR@SiO_2@QDs@SiO_2 functionalized with transferrin can efficiently target the cells and be taken up by the target cancer cells with a considerable quantity.

The internalization of PEGylated AuNR-QDs-Tf NPs was visually investigated by TEM. As expected, the NPs were avidly taken up by A549 cells. The cytosolic localization of the NPs inside the cells (Fig. 6) has shown that it may due to the receptor-mediated endocytosis (Chanda et al., 2009). A majority of the NPs found in cells showed no sign of aggregation and kept intact shape. This phenomenon could be due to the fact that the shell linked with abundant PEG ligands has provided excellent stability for the NPs so that they were less susceptible to enzymatic digestion. These results demonstrated the specific biomolecules such as transferrin functionalized AuNR@SiO_2@QDs@SiO_2 NPs can be used as luminescent reagent for fluorescence and dark-field co-localized imaging in vivo.

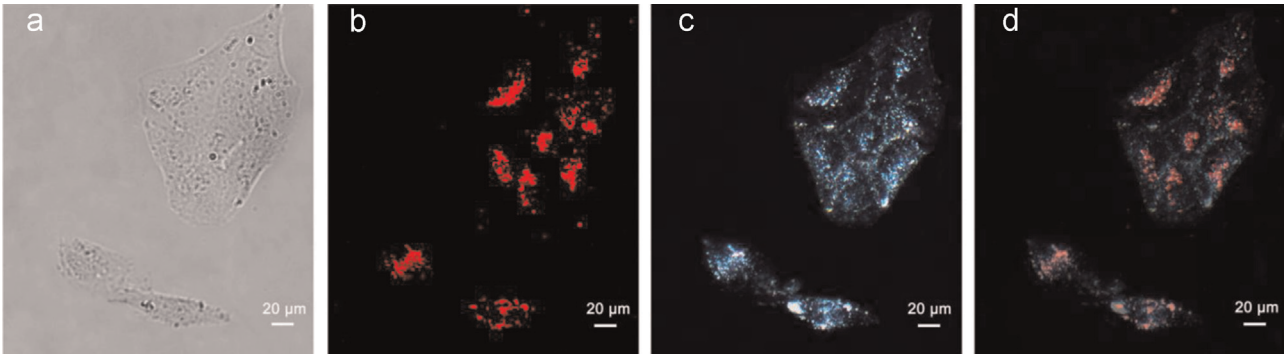

Fig. 7. (a) Bright-field image, (b) fluorescence image, (c) dark-field image and (d) overlaps image of A549 cells after 24 h incubation with PEGylatedAuNR-QDs-Tf. (For interpretation of the references to color in this figure, the reader is referred to the web version of this article.)

3.3. Dual modality co-localized cancer cell imaging

The transferrin-functionalized AuNR@SiO_2@QDs@SiO_2 NPs were further used for targeted imaging to A549 cells, which can express transferrin receptors in excess (Anabousi et al., 2006). After incubation for 24 h, the cells were imaged in dark field and fluorescence field respectively. Fig. 7c shows the dark-field scattering images of A549 cells labeled with PEGylated AuNR-QDs-Tf bio-conjugates. When exposed to white light, the cells showed an intense blue-green color, which could be attributed to the strong light scattering effect of AuNRs. The blue-green scattering signal originated from the transverse plasmon of AuNRs with a resonance frequency within the blue (green) region (Hu et al., 2009), but scattering at longitude plasmon resonance wavelength could not be visualized due to the sensitivity cutoff of the detector around 700 nm. Additionally, the corresponding fluorescence images (Fig. 7b) indicated that the NPs entered into the cytoplasm with a considerable quantity as strong red fluorescence emission could be seen. The overlap images (Fig. 7d) revealed that the blue-green signals from AuNRs and red fluorescence signals from QDs fitted well to each other. Control groups were carried out on A549 cells, HEK 293 cells and Hela cells using AuNR@SiO_2@QDs@SiO_2 and PEGylated AuNR-QDs-Tf respectively, as shown in Fig. S4. A low fluorescence/dark-field signal was observed after incubation with AuNR@SiO_2@QDs@SiO_2 NPs from A549 cells, and nearly no fluorescence/dark-field signal was detected while incubating PEGylated AuNR-QDs-Tf NPs with HEK293 cells. Furthermore, PEGylated AuNR-QDs-Tf was incubated with transferrin receptor antibody blocked Hela cells. The results have shown that there is no fluorescence/dark-field signal when PEGylated AuNR-QDs-Tf was incubated with the antibody blocked Hela cells, which was due to the blocking interaction between antibody and Hela cell transferrin receptors (Fig. S5). All the results clearly shown that the PEGylated AuNR-QDs-Tf bioconjugates were avidly uptake by the target cells as the red fluorescence and the blue-green scattering light were co-localized inside the cells, and successfully implemented targeted dual modal co-localized cell imaging.

4. Conclusions

In this study, we have fabricated a highly luminescent and biocompatible AuNR@SiO_2@QDs@SiO_2 nanocomposite and applied it in a dual-modalcancer targeted imaging. There are two achievements to be mentioned: 1) a large number of QDs were effectively immobilized on silica-modified AuNRs, with amphiphilic organosilica encapsulation and silicate deposition, the nanocompositenot only successfully avoided the FRET between QDs and AuNRs, but also kept intrinsic optical property of each integrated component. More importantly, with PEG capping and transferrin conjugation, the nanoprobe possessed low cytotoxicity and excellent cancer cell targeting ability; 2) the novel nanoprobe achieved both fluorescence and dark-field co-localized imaging simultaneously with high contrast, and provided a precise comparative analysis as well as elimination of the organism background interference. These results bring new insights into instructing nanocomposites for multi-modality image in bio-applications. Finally, with the thermal therapy ability of AuNRs (Huang et al., 2006), the as-prepared AuNR@SiO_2@QDs@SiO_2 nanoprobe is expected to be a promising candidate in disease diagnosis and therapy applications.

Supporting information

Experimental details for the preparation of CdSe/CdS/ZnS QDs and thiolated AuNR@SiO_2 substrates, zeta potential of PEG/transferrin modified NPs, PL/plasmonic stability of PEGylated AuNR-QDs-Tf NPs in DMEM, flow cytometric analysis of PEGylated AuNR-QDs-Tf NPs expression in A549 cells and HEK293 cells for 6 h, 12 h and 24 h, fluorescence/dark-field dual-modal imaging of A549 cells treated with AuNR@SiO_2@QDs@SiO_2 and HEK 293 cells incubated with PEGylated AuNR-QDs-Tf for 24 h, bi-exponential fitting parameter of the oil QDs and AuNR@SiO_2@QDs@SiO_2 nanocomposites, elemental analysis of AuNR-QDs-NH_2, AuNR-QDs-PEG and PEGylated AuNR-QDs-Tf NPs. This material is available free of charge via the Internet at http://pubs.acs.org.

Notes

The authors declare no competing financial interest.

Acknowledgment

We gratefully acknowledge financial support from the National Natural Science Foundation of China (21375043, 21175051 and 21305049).

Appendix A. Supplementary material

Supplementary data associated with this article can be found in the online version at http://dx.doi.org/10.1016/j.bios.2015.06.010.

References

Anabousi, S., Bakowsky, U., Schneider, M., Huwer, H., Lehr, C.M., Ehrhardt, C., 2006. In vitro assessment of transferrin-conjugated liposomes as drug delivery

systems for inhalation therapy of lung cancer. Eur. J. Pharm. Sci. 29, 367–374.
Bakalova, R., Zhelev, Z., Aoki, I., Masamoto, K., Mileva, M., Obata, T., Higuchi, M., Gadjeva, V., Kanno, I., 2008. Multimodal silica-shelled quantum dots: direct intracellular delivery, photosensitization, toxic, and microcirculation effects. Bioconjugate Chem. 19, 1135–1142.
Barreto, J.A., O'Malley, W., Kubeil, M., Graham, B., Stephan, H., Spiccia, L., 2011. Nanomaterials: applications in cancer imaging and therapy. Adv. Mater. 23, H18–H40.
Chen, H., Shao, L., Li, Q., Wang, J., 2013. Gold nanorods and their plasmonic properties. Chem. Soc. Rev. 42, 2679–2724.
Chanda, N., Shukla, R., Katti, K.V., Kannan, R., 2009. Gastrin releasing protein receptor specific gold nanorods: breast and prostate tumor avid nanovectors for molecular imaging. Nano Lett. 9, 1798–1805.
Ding, H., Yong, K.T., Roy, I., Pudavar, H.E., Law, W.C., Bergey, E.J., Prasad, P.N., 2007. Gold nanorods coated with multilayer polyelectrolyte as contrast agents for multimodal imaging. J. Phys. Chem. C 111, 12552–12557.
Foda, M.F., Huang, L., Shao, F., Han, H.Y., 2014. Biocompatible and highly luminescent near-infrared $CuInS_2$/ZnS quantum dots embedded silica beads for cancer cell imaging. ACS Appl. Mater. Interfaces 6, 2011–2017.
Fan, H.M., Olivo, M., Shuter, B., Yi, J.B., Bhuvaneswari, R., Tan, H.R., Xing, G.C., Ng, C. T., Liu, L., Lucky, S.S., Bay, B.H., Ding, J., 2010. Quantum dot capped magnetite nanorings as high performance nanoprobe for multiphoton fluorescence and magnetic resonance imaging. J. Am. Chem. Soc. 132, 14803–14811.
Gao, J., Gu, H., Xu, B., 2009. Multifunctional magnetic nanoparticles: design, synthesis, and biomedical applications. Acc. Chem. Res. 42, 1097–1107.
Gao, X., Cui, Y., Levenson, R.M., Chung, L.W.K., Nie, S., 2004. In vivo cancer targeting and imaging with semiconductor quantum dots. Nat. Biotechnol. 22, 969–976.
Gorelikov, I., Matsuura, N., 2007. Single-step coating of mesoporous silica on cetyltrimethyl ammonium bromide-capped nanoparticles. Nano Lett. 8, 369–373.
Gratton, S.E., Ropp, P.A., Pohlhaus, P.D., Luft, J.C., Madden, V.J., Napier, M.E., DeSimone, J.M., 2008. The effect of particle design on cellular internalization pathways. Proc. Natl. Acad. Sci. 105, 11613–11618.
Huang, X., Neretina, S., El-Sayed, M.A., 2009. Gold nanorods: from synthesis and properties to biological and biomedical applications. Adv. Mater. 21, 4880–4910.
Huang, L., Luo, Z., Han, H., 2012. Organosilane micellization for direct encapsulation of hydrophobic quantum dots into silica beads with highly preserved fluorescence. Chem. Commun. 48, 6145–6147.
Hu, R., Yong, K.T., Roy, I., Ding, H., He, S., Prasad, P.N., 2009. Metallic nanostructures as localized plasmon resonance enhanced scattering probes for multiplex dark-field targeted imaging of cancer cells. J. Phys. Chem. C 113, 2676–2684.
Huang, X., El-Sayed, I.H., Qian, W., El-Sayed, M.A., 2006. Cancer cell imaging and photothermal therapy in the near-infrared region by using gold nanorods. J. Am. Chem. Soc. 128, 2115–2120.
Ito, Y., Matsuda, K., Kanemitsu, Y., 2007. Mechanism of photoluminescence enhancement in single semiconductor nanocrystals on metal surfaces. Phys. Rev. B 75, 033309–033310.
Jin, Y., Jia, C., Huang, S.W., O'Donnell, M., Gao, X., 2010. Multifunctional nanoparticles as coupled contrast agents. Nat. Commun. 1, 41–42.
Jin, Y., Gao, X., 2009. Plasmonic fluorescent quantum dots. Nat. Nanotechnol. 4, 571–576.
Jun, B.H., Hwang, D.W., Jung, H.S., Jang, J., Kim, H., Kang, H., Kang, T., Kyeong, S., Lee, H., Jeong, D.H., Kang, K.W., Youn, H., Lee, D.S., Lee, Y.S., 2012. Ultrasensitive, biocompatible, quantum-dot-embedded silica nanoparticles for bioimaging. Adv. Funct. Mater. 22, 1843–1849.
Jana, N.R., Earhart, C., Ying, J.Y., 2007. Synthesis of water-soluble and functionalized nanoparticles by silica coating. Chem. Mater. 19, 5074–5082.
Koole, R., van Schooneveld, M.M., Hilhorst, J., de Mello Donegá, C., Hart, D.C., van Blaaderen, A., Vanmaekelbergh, D., Meijerink, A., 2008. On the incorporation mechanism of hydrophobic quantum dots in silica spheres by a reverse microemulsion method. Chem. Mater. 20, 2503–2512.
Li, M., Cushing, S.K., Wang, Q., Shi, X., Hornak, L.A., Hong, Z., Wu, N., 2011. Size-dependent energy transfer between CdSe/ZnS quantum dots and gold nanoparticles. J. Phys. Chem. Lett. 2, 2125–2129.
Lu, Z., Gao, C., Zhang, Q., Chi, M., Howe, J.Y., Yin, Y., 2011. Direct assembly of hydrophobic nanoparticles to multifunctional structures. Nano Lett. 11, 3404–3412.
Liu, N., Prall, B.S., Klimov, V.I., 2006. Hybrid gold/silica/nanocrystal-quantum-dot superstructures: synthesis and analysis of semiconductor-metal interactions. J. Am. Chem. Soc. 128, 15362–15363.
Li, X., Qian, J., Jiang, L., He, S., 2009. Fluorescence quenching of quantum dots by gold nanorods and its application to DNA detection. Appl. Phys. Lett. 94, 063111–063112.
Michalet, X., Pinaud, F.F., Bentolila, L.A., Tsay, J.M., Doose, S., Li, J.J., Sundaresan, G., Wu, A.M., Gambhir, S.S., Weiss, S., 2005. Quantum dots for live cells, in vivo imaging, and diagnostics. Science 307, 538–544.
Mulder, W.J.M., Koole, R., Brandwijk, R.J., Storm, G., Chin, P.T.K., Strijkers, G.J., de Mello Donegá, C., Nicolay, K., Griffioen, A.W., 2005. Quantum dots with a paramagnetic coating as a bimodal molecular imaging probe. Nano Lett. 6, 1–6.
Nepal, D., Drummy, L.F., Biswas, S., Park, K., Vaia, R.A., 2013. Large scale solution assembly of quantum dot gold nanorod architectures with plasmon enhanced fluorescence. ACS Nano 7, 9064–9074.
Nikoobakht, B., El-Sayed, M.A., 2003. Preparation and growth mechanism of gold nanorods using seed-mediated growth method. Chem. Mater. 15, 1957–1962.
Nativo, P., Prior, I.A., Brust, M., 2008. Uptake and intracellular fate of surface-modified gold nanoparticles. ACS Nano 2, 1639–1644.
Pérez-Juste, J., Pastoriza-Santos, I., Liz-Marzán, L.M., Mulvaney, P., 2005. Gold nanorods: synthesis, characterization and applications. Coord. Chem. Rev. 249, 1870–1901.
Peng, B., Li, Z.P., Mutlugun, E., Mart´ınez, P.L.H., Li, D., Zhang, Q., Gao, Y., Demir, H.V., Xiong, Q.H., 2014. Quantum dots on vertically aligned gold nanorod monolayer: plasmon enhanced fluorescence. Nanoscale 6, 5592–5598.
Pons, T., Medintz, I.L., Sapsford, K.E., Higashiya, S., Grimes, A.F., English, D.S., Mattoussi, H., 2007. On the quenching of semiconductor quantum dot photoluminescence by proximal gold nanoparticles. Nano Lett. 7, 3157–3164.
Resch-Genger, U., Grabolle, M., Cavaliere-Jaricot, S., Nitschke, R., Nann, T., 2008. Quantum dots versus organic dyes as fluorescent labels. Nat. Methods 5, 763–775.
Song, S., Qin, Y., He, Y., Huang, Q., Fan, C., Chen, H.Y., 2010. Functional nanoprobes for ultrasensitive detection of biomolecules. Chem. Soc. Rev. 39, 4234–4243.
Shi, W., Zeng, H., Sahoo, Y., Ohulchanskyy, T.Y., Ding, Y., Wang, Z.L., Swihart, M., PNA, Prasad, 2006. General approach to binary and ternary hybrid nanocrystals. Nano Lett. 6, 875–881.
Tian, Q., Hu, J., Zhu, Y., Zou, R., Chen, Z., Yang, S., Li, R., Su, Q., Han, Y., Liu, X., 2013. Sub-10 nm Fe_3O_4@$Cu_{2-x}S$ core–shell nanoparticles for dual-modal imaging and photothermal therapy. J. Am. Chem. Soc. 135, 8571–8577.
Wu, C., Xu, Q.H., 2009. Stable and functionable mesoporous silica-coated gold nanorods as sensitive localized surface plasmon resonance nanosensors. Langmuir 25, 9441–9446.
Wang, J., Tian, S., Petros, R.A., Napier, M.E., DeSimone, J.M., 2010. The complex role of multivalency in nanoparticles targeting the transferrin receptor for cancer therapies. J. Am. Chem. Soc. 132, 11306–11313.
Xia, H.X., Yang, X.Q., Song, J.T., Chen, J., Zhang, M.Z., Yan, D.M., Zhang, L., Qin, M.Y., Bai, L.Y., Zhao, Y.D., 2014. Folic acid-conjugated silica-coated gold nanorods and quantum dots for dual-modality CT and fluorescence imaging and photothermal therapy. J. Mater. Chem. B 2, 1945–1953.
Xia, Y., Song, L., Zhu, C., 2011. Turn-on and near-infrared fluorescent sensing for 2,4,6-trinitrotoluene based on hybrid gold nanorod-quantum dots assembly. Anal. Chem. 83, 1401–1407.
Zhu, Y., Li, Z., Chen, M., Cooper, H.M., Lu, G.Q., Xu, Z.P., 2012. Synthesis of robust sandwich-like SiO_2@CdTe@SiO_2 fluorescent nanoparticles for cellular imaging. Chem. Mater. 24, 421–423.